Experimental investigation on the effect of Leading Edge Tubercles on the Performance of Marine Propellers in fully wet condition

Massimo Falchi[a], Fabrizio Ortolani[a,*], Weichao Shi[b], Callum Stark[b], Giovanni Aloisio[a], Silvano Grizzi[a], Giulio Dubbioso[a]

[a] *CNR-INM, via del Vallerano 139, 00128 Roma, Italy*
[b] *Naval Architecture, Ocean and Marine Engineering, University of Strathclyde, Glasgow, UK*

Abstract

Leading edge tubercles (LET) is an attractive passive flow control solution that has been proved to enhance the hydrodynamic performance and efficiency of lifting surfaces adopted in many engineering areas. Nonetheless, their industrial application in control and propulsion devices of marine vehicles is still at the beginning. To move further steps ahead, a preliminary experimental campaign for a five bladed Wageningen B–screw propeller modified with three different configurations of leading edge tubercles was carried out in cavitation free conditions. In particular, the propellers were tested in open water conditions in straight and oblique flow at incidences of 10° and 20°, with the aim to study the effects of LET during steady and moderate unsteady conditions. The propellers are tested at two different chord Reynolds numbers in order to investigate their applicability also to small autonomous marine vehicles. The analysis proved that suitable layout of tubercles can enhance the hydrodynamic efficiency in axial symmetric flow while reducing undesired effects caused by operation in off–design.

Keywords: leading edge tubercles, propeller performance, propeller in oblique flow, bio inspired propeller blade design

1. Introduction

Modern design procedures of the propulsion device of a marine platform need to be improved in order to comply with more stringent requirement imposed by international regulation for the reduction of the environmental pollution (gas emissions to air and noise), safety during operations and maintenance costs. This issue fostered a growing attention to realistic operative conditions, including off–design and environmental interaction (waves, wind). In this context, state of the art optimization techniques, implemented in multi–input and multi–objective optimization paradigm, were proven to be feasible for the design of a propeller in waves accounting for nominal wakes at different phases of the waves (Grigoropoulos et al., 2017). Alternatively, the development of novel technological solutions can be conceived from inspiration of biological systems. A flourishing topic that has been profoundly grabbed the attention of research in a myriad of applications, ranging from flying machines

*Corresponding author.
Email address: fabrizio.ortolani@cnr.it (Fabrizio Ortolani)

This is a peer reviewed, accepted author manuscript of the following research article: Falchi, M., Ortolani, F., Shi, W., Stark, C., Aloisio, G., Grizzi, S., & Dubbioso, G. (2022). Experimental investigation on the effect of leading edge tubercles on the performance of marine propellers in fully wet condition. Ocean Engineering, 255, [111249]. https://doi.org/10.1016/j.oceaneng.2022.111249

to race bicycle wheels, regarded the unique flow control qualities provided by the leading edge tubercles that characterize the pectoral flipper of the whale (Fish and Battle, 1995) or the ears of the free–tail Brazilian bat (Petrin et al., 2018), see Figures 1 and 2, respectively. The earlier conjectures on the enhancement provided by these protuberances were suggested by the superior maneuvering capabilities of the Humpback whale while catching the prey in contrast to similar big mammals characterized by smooth fins (Fish and Battle, 1995). Subsequent wind tunnel measurements of lift and drag on a scaled humpback fins with smooth and scalloped leading edge (Miklosovic et al., 2004, 2007) confirmed the enhancement on hydrodynamic loads and efficiency for the latter configuration. The study highlighted both an increase of hydrodynamic efficiency in the post–stall regime (enhancement of lift in contrast to drag) and a softer transition to the stalled regime. Detached Eddy Simulations (DES) (Pedro and Kobayashi, 2008) and PIV (Particle Image Velocimetry) measurements performed on analogous scalloped wing (Stanway, 2008) revealed the onset of additional vortical structures in correspondence of the protuberances and their beneficial effect to the evolution of the flow with respect to the equivalent smooth surface. Specifically, the tubercles give rise to a pairs of counter rotating vortices (see Figure 3) that play a dual role. On one side, they energize the boundary layer, delaying the onset of stall and pushing the separation point further back on the surface on the sections in the crests. On the other, these vortices induce a velocity that increases the incidence angle in the crests and, hence, act to anticipate the stall keeping it confined in the troughs. Moreover, in finite–wing configurations, the vortex pairs act to compartmentalize the flow, thus reducing the losses associated with the tip vortex flow. Significant amount of systematic investigations on full–span and finite span wings, carried out both by experiments and viscous flow simulations employing different turbulence modeling paradigms (based on Reynolds averaging, Detached and Large Eddy Simulations), evidenced the strict relationship between the behavior of the vortex pairs and tubercle geometry to efficiency enhancement: specifically, this is achieved with the increase of amplitude–to–wavelength ratio of the tubercle (where the wavelength is the spatial distance between two consecutive crests).

Figure 1: Leading Edge Tubercles of whale flippers

Figure 2: Leading Edge Tubercles on tail-free Brazilian Bat

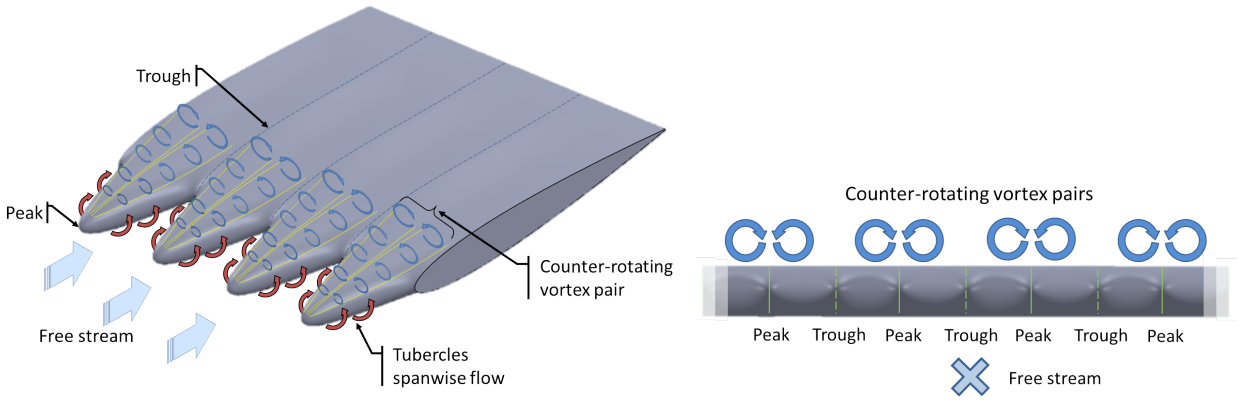

Figure 3: Basic flow mechanism induced by leading edge tubercles (adaptation from (Shi et al., 2019a))

The interaction of the tubercle vortex and the boundary layer have consequences on unsteady performance and its radiated noise. In fact, the vortex pairs acts to weaken the coherency of the structures detached past the foil: on one side, the trough of the tubercle acts to stabilize the separated flow and on the other, the acceleration and compartmentalization of the vortex pair to the flow that delay the separation, act to weaken the turbulent perturbation of the boundary layer and, consequently, tonal and broadband noise (Lau et al., 2012, 2013; Lacagnina et al., 2021). Moreover, these mechanisms act to mitigate the fluctuations of the loads and hysteresis cycle during unsteady motions, in particular during the dynamic stall regime (Hrynuk and Bohl, 2020; Zhang et al., 2020). The *LET* provided also potential benefits in cavitating flow regime. Specifically, experimental research carried out on marine rudder foils evidenced that the onset of cavitation was triggered in troughs at smaller incidence angle rudder with respect to the smooth geometry. However, at highest angle of attack, less cavitation volume was produced (Weber et al., 2010; Custodio et al., 2018). Large Eddy Simulations for a full span rectangular wing highlighted that the suppression of cavitation was more efficient, analogously to the cavitation free condition, with the increase of the amplitude–to–drag ratio up to 30%. Moreover, at the highest angle of attack (24°) the pressure pulses on the suction side were reduced by almost 60% with respect to the basic configuration (Li et al., 2021). As also observed by an analogous numerical study based on *LES*, the reduction of the scales of the cloud cavitation in correspondence of the trailing edge was ascribed to the effect of the vortex pairs (Li et al., 2020).

The benefits obtained for full and finite span wings have been also observed by systematic investigations performed on rotating devices, in particular power generation devices (wind and water turbines) (Bai et al., 2016; Zhang and Bi, 2012; Ibrahim et al., 2015; Ke et al., 2022; Shi et al., 2016a,b, 2019b) and aeronautic propellers (Butt and Talha, 2019; Asghar et al., 2020). In general, these studies confirmed that the increase of the amplitude and reduction of the wavelength was the most influencing parameter of the tubercle geometry to achieve efficiency gains. Reduction of load fluctuations for tidal turbine equipped with *LET* operating near free surface and in cavitating regimes were observed in (Shi et al., 2016b, 2019b). It is worth noting that the experiments for tidal turbine (Shi et al., 2016a) and aeronautic propellers (Asghar et al., 2020) further explored

hybrid blade configurations, obtained with localized inclusion of the LET along the span (root, mid and tip). In particular, the acoustic survey reported in (Asghar et al., 2020), confirmed the effectiveness in noise abatement of the tubercles for both broadband and tonal components (due to weakening of the tip vortices).

The potential benefit of leading edge tubercles in terms of efficiency, mitigation of unsteady loads and noise make them promising for the implementation on control and propulsion devices of marine vehicles. In fact, efficiency of rudder is fundamental for providing both directional stability to the ship under the action of waves and wind and for performing fast and reactive maneuvers. Propeller blades, operating in a complex unsteady flow caused by the spatial and temporal variability characterizing the wake past the hull, need to be optimized to deliver the propulsive power with minimum amount of energy. During maneuvers or motion in waves, the blades, optimized for the inflow in ideal condition (straight ahead advancement in calm water), are subjected to a different angle of attack. As a consequence, the mean loads and their fluctuation as well as the onset, development and features of the cavitation pattern can be altered (Ortolani and Dubbioso, 2019b,a), affecting the structural reliability of the propulsive components (Ortolani et al., 2018; Dubbioso and Ortolani, 2020) or emitted noise (Dubbioso et al., 2020). Moreover, unmanned autonomous vehicles are rapidly expanding for various mission profile at sea (as well as land and air). The prerogative of these vehicles is autonomy and stealthiness and typically they perform tight maneuvers at low speed. Therefore, rudders and propellers can be affected by regions of laminar or transitional flow, and passive control provided by tubercles or other bio–mimetic devices are actively studied for future biologically inspired Autonomous Underwater Vehicles (Fish, 2020).

In this framework, specific research on the application of leading edge tubercles mainly regarded rudders and marine propellers. In addition to the survey on marine rudder cavitation (Weber et al., 2010; Custodio et al., 2018), simulations based on the solution of the Reynolds averaged Navier–Stokes equations ($RANSE$) and experiments in the towing tank further showed that non–homogeneous distributions of tubercles resembling those of the pectoral fin were superior in the post–stall regime with respect to homogeneous distributions (Shanmukha Srinivas et al., 2018). From the realistic distribution of tubercles, twin protuberance layout was conceived and further experimental and numerical simulations based on flow transition sensitive model and $RANSE$ clarified the role of their spacing to maximize their hydrodynamic efficiency in the post–stall regime (Kant and Bhattacharyya, 2020). The performance of a tubercled rudder installed in behind the hull and in the propeller wake has been considered for the first time in (Shin et al., 2019) for the KRISO ship model by means of experiment in the towing tank and $RANSE$ simulations with discretized rotating propeller. The study stressed that the modified rudder did not worsen self–propulsion performance of the vessel at zero deflection angle while it was markedly superior in deflected conditions up to large incidences in the post stall regime. While most of the studies focused on the hydrodynamic loads and modification of wall flow due to the vortex pairs generated by tubercles, (Troll et al., 2021) analyzed their effect on the dynamics of the wake past a marine rudder by Improved Delayed Detached Eddy Simulations ($IDDES$). The system of vortex pairs interfere with the vorticity shed past the trailing edge and the compartmentalization of the flow alters the distribution magnitude and vorticity

of the wake system. In particular, it was showed that the vortex pairs act to destroy the shed wake and weaken the circulation carried by the tip vortex. As a results, the tip vortex can experience a different trajectory and dissipates at a different rate and/or experiences onset of destabilization modes. These aspects are of utmost importance in marine hydrodynamic applications, given the strict relation of the turbulent structures in the wakes with noise sources (Ianniello et al., 2014).

The application of leading edge tubercles to propulsive devices were attractive, although most of the studies were not carried out in a systematic fashion. A pioneering investigation concerned a systematic analysis of the LET to the duct of a ducted–propeller system by $RANSE$ simulations (Stark et al., 2021a). In particular, the analysis converged toward an optimal configuration of the duct that allowed to maximize the thrust and limit the separation region in the suction side of the duct itself. Moreover, $IDDES$ computations for the optimal LET geometry pointed out that the vortex pairs, generated in the inner side of the duct, modified the inflow to the blade and, consequently, the load developed by the blades (Stark and Shi, 2021a). In general, it was found that propeller loads (thrust and torque) were reduced in contrast to increase of thrust of the duct that resulted in efficiency enhancement for almost the whole range of advance coefficient considered. Moreover, the vortex pairs profoundly interacted with the wake shed from the duct and propeller wake system, enhancing the suppression of noise emission for this modified system.

Specific investigations on marine propellers were performed considering both the cavitation–free and cavitating flow in open water conditions exclusively by means of numerical techniques. However, all the available studies considered a single modification of the blades with leading edge tubercles with the exception of (Stark et al., 2021b). Briefly, in cavitation–free conditions, three bladed propeller (Ibrahim and New, 2015b,a), four bladed propeller (Naveen et al., 2018; Arifin and Felayati, 2021) and five blade propeller (Stark and Shi, 2021b) were considered. These studies evidenced that the tubercled propeller developed higher thrust and torque and penalization of hydrodynamic efficiency in the low–to–medium advance coefficient range. In cavitating conditions, a preliminary investigation for a five bladed propeller (Stark and Shi, 2021b) highlighted that the tubercles act to reduce the vapor volume and increment the efficiency in deep cavitation regime (heavy propeller loading). These results were corroborated for the case of a ducted, four bladed Kaplan propeller (Stark et al., 2021b). Moreover, in this case, two wave profiles were analyzed and it was shown that the reduction of the wavelength was the best solution among most of the conditions considered. Otherwise, the configuration with the highest wavelength was more beneficial in very heavy loading conditions due to the presence of the tubercle close to the root. Finally, the preliminary investigation for a three bladed propeller modified with a single tubercle per blade highlighted the compartmentalization effect of the vapor volume due to the tubercle in contrast to a larger production of the cavity in certain operating conditions (Charalambous and Eames, 2019).

An alternative biomimetic solution applied to a marine propeller was proposed in (Zhu and Gao, 2021). Specifically, the shape of the blade of the MAU–80 and a five bladed Wageningen B–series propeller was modified according to the chord and camber of the wings of birds (owl, teal, seagull and merganser). The analysis, carried out by means of $RANSE$ simulations, showed benefits in terms of efficiency and tip vortex

strength mitigation, useful to suppress the undesired effect of tip vortex cavitation and associated noise.

These works showed a partial overview of the potential benefit of *LET* on marine propeller performance, because they focused on a single specific configuration and always considered the ideal condition in open water and axial–symmetric flow. For these reasons, research on the topic is at least at its beginning and further investigation is indisputably warranted. On this basis, in the present work a preliminary experimental survey for a benchmark propeller series introduced in (Stark and Shi, 2021b) is presented with three different *LET* configurations in open water condition both in axial–symmetric and oblique flows at incidence of 10° and 20°. According to the authors knowledge, the investigation of incident flow has not yet been investigated in general for propeller and turbines, although it can be considered an idealized realistic operative condition in off–design. In these tests, the propeller are tested at the CNR–INM towing tank considering two different chord Reynolds Number in order to investigate the relative hydrodynamic enhancement provided by the tubercle in the presence of laminar or transitional conditions. The results are reported in terms of propulsive components (thrust and torque) and in–plane forces (i.e. vertical and lateral forces). This study confirms the fact that the performance of the propellers depend on the ratio between amplitude and the wavelength of the tubercle in a different fashion with respect to findings on low solidity rotors (featuring blades with high aspect ratio). Moreover, a promising result is that the leading edge tubercle configuration that boosted the hydrodynamic efficiency in axial symmetric flow also exhibited attractive performance in oblique flow in terms of reduction of thrust and torque overloading and amplification of maneuvering force. Although this benchmark is limited, it can also be useful for *CFD* validation, since it is not yet assessed for these particular bio–inspired technology.

2. Test Case and Experimental Set–up

The baseline geometry is a Wageningen B–Screw propeller with modified sections based on the NACA0012 foils (Stark and Shi, 2021b). The geometric characteristics of the baseline propeller are listed in Table 1. The geometry of the tubercles is developed by variation of two parameters, namely amplitude A_{LE} and wavelength λ. Two wavelengths and wave heights with uniform distribution along the span of the blade were considered. The modified propellers are defined in Table 2 according to the characteristics of the tubercle geometry and are shown in Figure 5. The inset on the side of the blades compares the original and modified leading edge by the tubercle. The amplitudes of the tubercles correspond to 5% and 10% and of the chord, whereas the wavelength is 10% and 20% of the span.

Table 1: Geometric characteristics of the baseline propeller model

MODEL AND PROPELLER DATA	
Blade Number Z	5
Expanded Area Ratio A_E/A_O	0.6
Pitch Diameter Ratio P/D	1.2
Chord @0.7 Diameter Ratio C/D	0.237
Diameter D	0.24
Hub/Diameter Ratio	0.2
Rake	0°
blade section	NACA-0012

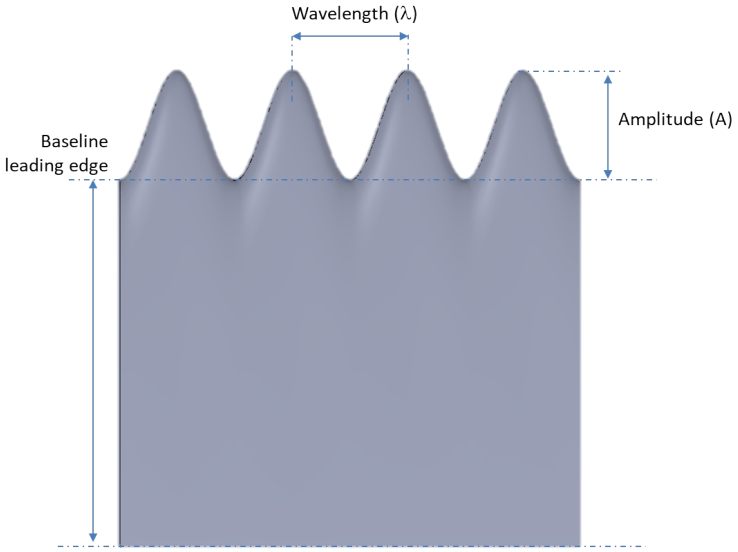

Figure 4: Definition of tubercle parameter

Table 2: Features of *LET* for modified propellers

P0	Baseline
P1	high amplitude (10% chord), high wavelength (20% span)
P2	low amplitude (5% chord), high wavelength (20% span)
P3	low amplitude (5% chord), low wavelength (10% span)

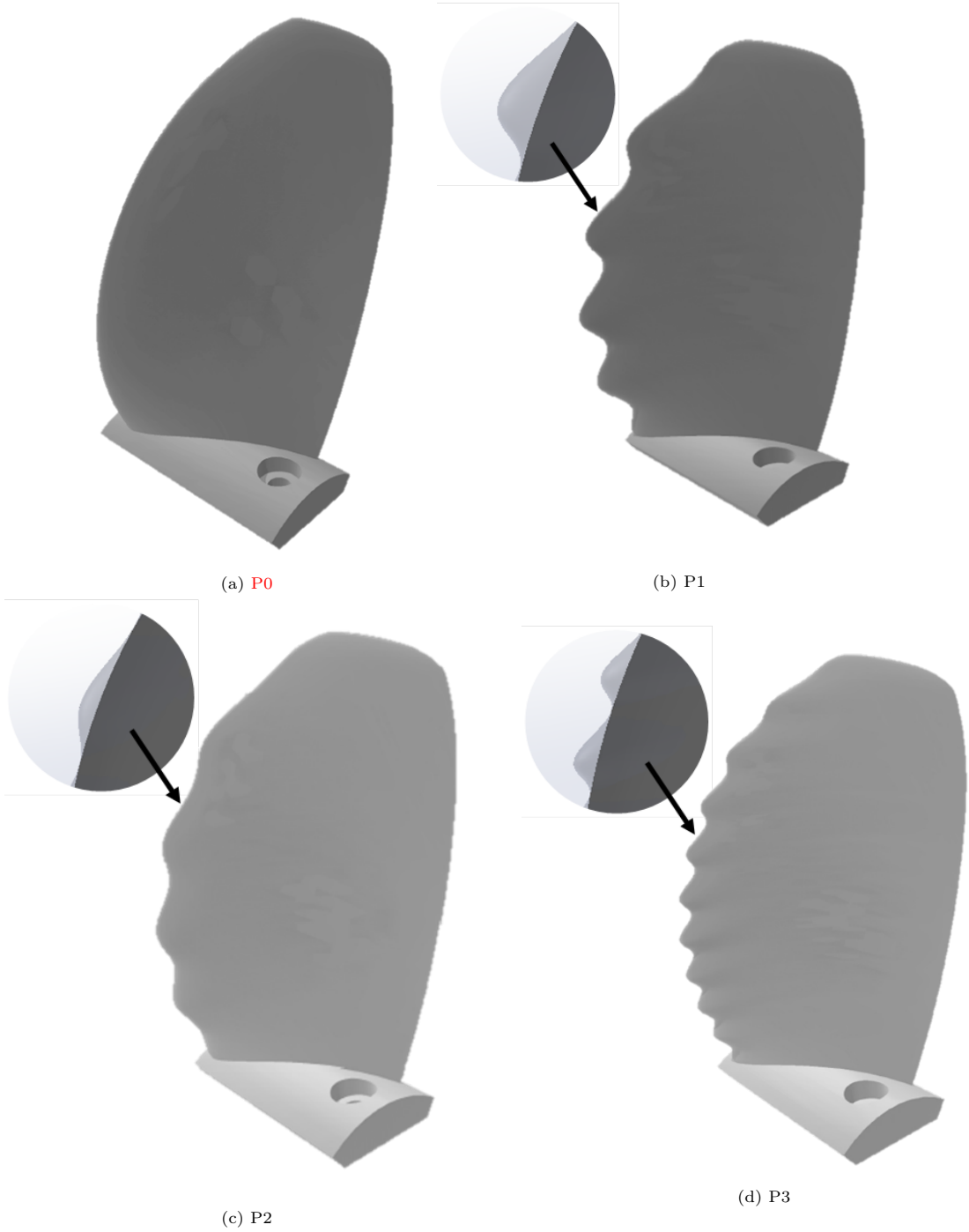

(a) P0

(b) P1

(c) P2

(d) P3

Figure 5: Propeller series and detailed view of tubercles definition

The propellers were tested at two different Reynolds numbers $Re_c = 1.0x10^5$ and $2.5x10^5$ referred to the section at radial position 0.7 and defined as follows:

$$Re_c = \frac{V_{0.7}c_{0.7}}{\nu} = c_{0.7}\frac{\sqrt{{V_A}^2 + (0.7\pi ND)^2}}{\nu} \tag{1}$$

where ν is the kinematic viscosity of the water, N and D are the propeller rate of revolution and the propeller diameter, V_A is the free stream velocity (equal to the advance speed of the carriage) and $c_{0.7}$ is the chord length at 70% of the blade span. The two different regimes are selected to investigate the sensitivity of the tubercles to Reynolds number. The lower value has been set with the aim to emphasize the tubercle effect to trigger transition from laminar to turbulence regime. This aspect has been poorly inspected in literature and can be useful for some applications in small unmanned vehicles, where the increased efficiency of the propulsors is critical for the admissible payload or mission profile.

The experiments were carried out in the towing tank of CNR–INM. The experimental setup is sketched in figure 6: the propeller is installed on the H29 dynamometer from Kempf & Remmers with full scale values of 400 N for the thrust, 15 Nm for the torque and a maximum revolution speed of 60 RPS. The dynamometer is constrained to the carriage (that is not visualized) that runs at the advance speed V_A. According to the *ITTC* Procedure and guidelines (ITTC, 2014), the propeller axis was set at a distance of two propeller diameters from the free surface. The dynamometer was inclined in the vertical plane by tilt angle β to perform oblique flow tests in order to obtain a broader description of the behavior of the selected propellers and shed light on their different hydrodynamic performance. To this purpose, the shaft was also equipped with a transducer for the lateral loads. Essentially, this device consists of strain gauges placed at the propeller shaft within the sting case of the dynamometer at a distance d equal to 420 mm from the propeller plane. Since the lateral forces are monitored at the dynamometer sting that does not coincide with the propeller plane, the lateral and vertical force measurements include also the effect of in–plane moments generated by the asymmetry of the load during the cycle experienced by the blades in oblique flow (see, for example (Ortolani et al., 2015)). This is sketched for the sake of clarity in the inset at the bottom of figure 6 for the specific case experienced in the present tests: the vertical force Fz arises from the imbalance of the vertical force developed by the blades during the upstroke and downstroke phases of the cycles (blue arrows). Consistently, the thrust is also asymmetric during the phases of the cycle and a yaw moment M_Z is developed. M_Z gives onset to a reaction to the measurement point in horizontal plane that sums up to the hydrodynamic contribution due to the asymmetric distribution of inflow induced by the deflection of the propeller slipstream. The global uncertainty, evaluated during the calibration of the instrument in dry conditions and on the past experience (so comprehensive of type A and B uncertainty), is 0.39% for the thrust and 0.41% for the torque.

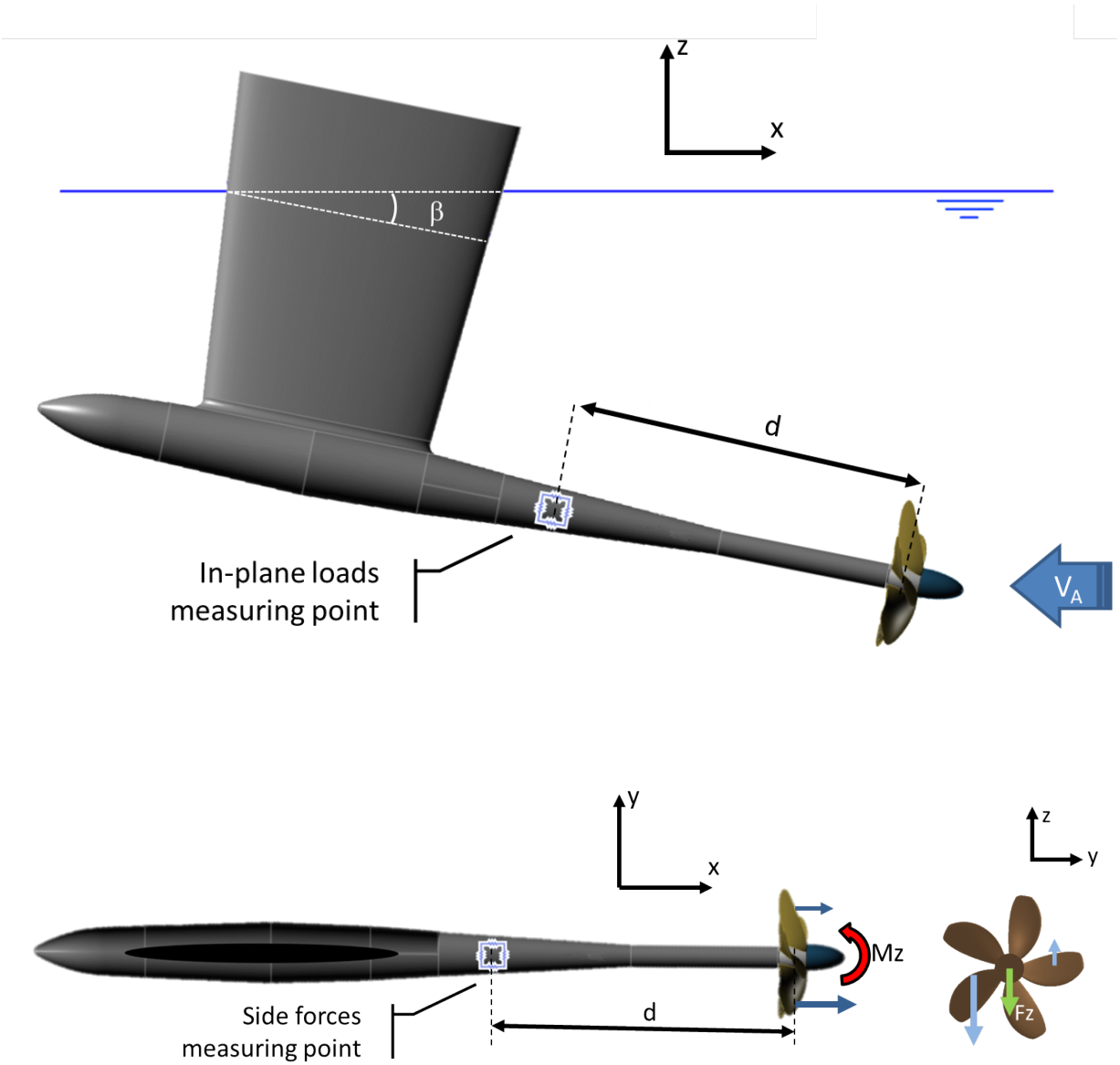

Figure 6: Experimental set–up for the open water tests

3. Results

The results are presented in terms of the characteristics propeller loads, namely propulsive (thrust and torque) and in–plane, and efficiency. The thrust T (and in–plane loads) and torque Q are presented in non dimensional form as usual, namely:

$$K_T = \frac{T}{\rho N^2 D^4} \qquad K_Q = \frac{Q}{\rho N^2 D^5} \tag{2}$$

where ρ is density, N is the propeller rate of revolution and D is the propeller diameter. As usual, the operating condition of the propeller is identified by the advance coefficient J:

$$J = \frac{V_A}{ND} \tag{3}$$

The efficiency η is defined as:

$$\eta = \frac{JK_T}{2\pi K_Q} \tag{4}$$

3.1. Open Water Condition at $0°$

The open water characteristics of the selected propellers are reported in Figure 7 for the two Reynolds number. In order to highlight the discrepancies with respect to the baseline geometry, the absolute difference of the characteristics K_T, K_Q and η are showed in Figure 8 for the lower (solid) and higher (dashed) Re_c. The modified propellers develop higher thrust and torque in the whole range of advance coefficient with respect to the baseline, see in particular Figures 8a and 8b. Propeller $P1$, characterized by high wavelength and high amplitude, experiences the most similar behavior with respect to the baseline. Conversely, LET characterized by low amplitude and high wavelength ($P2$) gives rise to the largest differences with respect to $P0$. Model $P3$ is almost intermediate with respect to the previous modified models. Figure 8 also shed light on the effects of tubercles for the different propeller loading conditions. In fact, the discrepancy of K_T always decreases with the increase of J for high amplitude and high wavelength tubercles ($P1$), it is almost constant for low amplitude and high wavelength tubercles ($P2$) and it is increasing for low amplitude and low wavelength tubercles ($P3$). On the other hand, the raise of K_Q is gradually smoothed with the increase of the advance coefficient for all modified geometries in the laminar regime: the trend is non linear, i.e. it drops faster for heavy propeller loading ($J < 0.4$) and then it evolves smoothly. At $Re = 2.5 \cdot 10^5$ these trends are smoothed with the exception of low frequency and low amplitude LET that cause the torque discrepancy to be almost constant. The efficiency of the modified propellers is worse than the baseline model for $J < 0.9$, see Figures 7 and 8c. This is due to the fact that the increase of absorbed torque is greater than the generated thrust. In this case, the model characterized by low amplitude and high wavelength tubercles is the farthest from $P0$. On the other hand, for $J > 0.9$ the tubercles yield an increase of efficiency. Note that in this working range model $P2$ is the most efficient solution. Moreover, in the turbulent regime the maximum efficiency seems to be kept for a larger interval of J with respect to the other models.

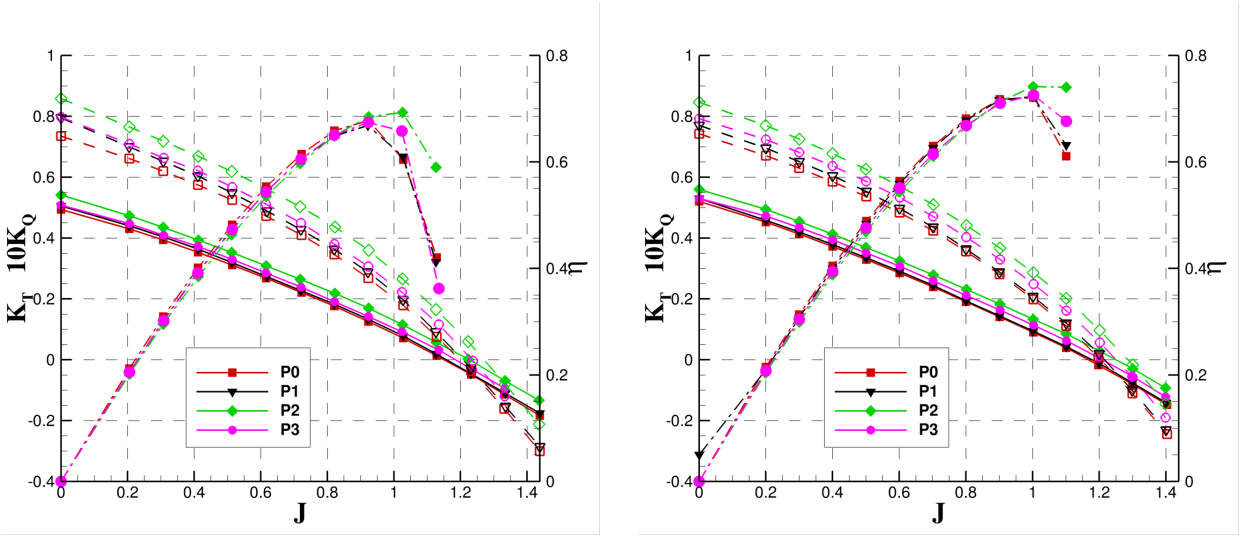

(a) $Re_c = 1.0x10^5$ (b) $Re_c = 2.5x10^5$

Figure 7: Open water characteristics. Solid: K_T; dashed: $10K_Q$; dot–dashed: η

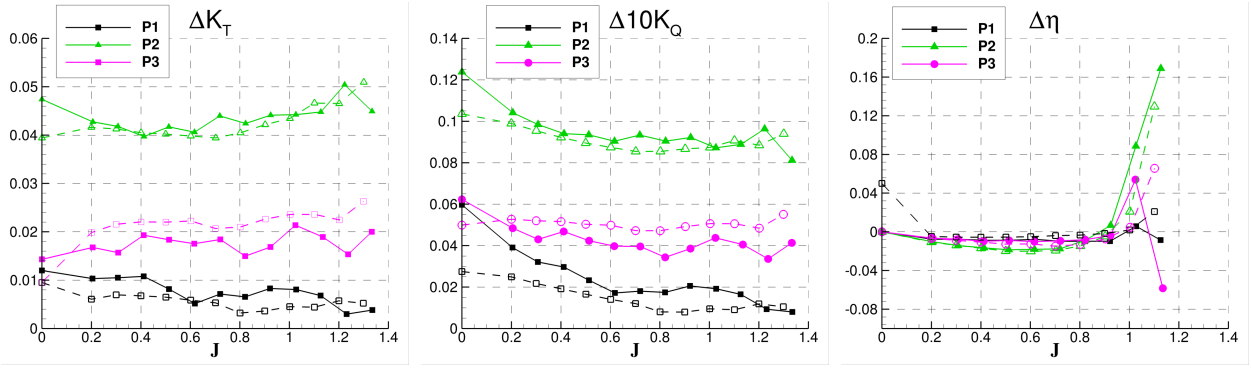

(a) Thrust (b) Torque (c) efficiency

Figure 8: Absolute discrepancy with respect to baseline propeller. Solid: $Re_c = 1.0x10^5$; dashed: $Re_c = 2.5x10^5$

Synthesis with results available in literature

It is constructive to synthesize the present results with documented outcomes for aeronautic and available propellers in order to draw new guidelines to broaden the present benchmark test case. First of all, a preliminary numerical investigation for this benchmark test case has been carried out in (Stark and Shi, 2021b), only for $P3$ and the baseline models. The computations, performed in the range of $0.2 < J < 0.9$, captured the trend of efficiency (increasing with J but lower than the baseline), the higher and lower generation torque and thrust respectively, for the modified model with respect to original leading edge.

The results of the present experimental campaign qualitatively agree with those obtained by the numerical investigation for a three bladed propeller with a single LET configuration (Ibrahim and New, 2015b,a). In particular, the computations evidenced that the thrust and torque were higher than the baseline propeller. Although the efficiency was exacerbated, it featured a monotonically increasing trend up to exceed the baseline value in correspondence of $J = 0.9$ (close to the sign inversion obtained in the actual experiments). Conversely,

different results are documented by the numerical investigation in (Naveen et al., 2018) for a modified version of the INSEAN E779A propeller. The simulations revealed a slight increase of thrust in contrast of a considerable of torque to yield an almost constant efficiency gain for the whole range of J. The computational analysis by $IDDES$ (Stark et al., 2021b) for a ducted propeller with leading edge bumps characterized by amplitudes of 10% of the chord and two different wavelength, confirmed the increase of thrust and torque and the reduction of efficiency for $0.2 < J < 0.55$ (medium–heavy loading condition typical for this kind of propulsors). Moreover, the efficiency of the modified models marginally improved with the reduction of wavelength. The results of the present investigation do not confirm the outcome of the computational investigation for aeronautic propellers reported in (Butt and Talha, 2019). The study considered four LET tubercles, obtained by the combination of two tubercle amplitude (10% and 20% of the chord) and two wavelength. All the modified propellers improved their efficiency. In particular, the largest efficiency gains were obtained by increasing the tubercle amplitude–to–wavelength ratio. However, thrust and torque data are not available and a comparison, at least qualitative, with the present ones can not be performed. In this regard, the computational analysis described in (Joshi et al., 2020), carried out for aeronautic propeller similar to (Butt and Talha, 2019) for only a single modified geometry, confirmed that the leading edge tubercles improve the efficiency for all the range of advance coefficient tested, although the thrust and torque were lower with respect to the original configuration. These outcomes qualitatively confirm the findings drawn for wings and tidal turbines (Shi et al., 2019b). On the contrary, the results for the present benchmark confirmed the gain of efficiency from high to low wavelength (models $P3$ and $P2$, respectively), while the worsening from low to high amplitude shape (models $P2$ and $P1$, respectively).

The CFD analysis presented in (Asghar et al., 2020) investigated the effect of different locations of two tubercle configurations with equal amplitude of the wave profile (12.5% of the chord) with constant and variable spacing (i.e., constant spacing–to–chord ratio). In this case, the efficiency of the modified propellers with respect to the smooth leading edge resembled the same results of the present investigation for certain spacing distributions (tubercles at the tip) and highlighted that the tubercles at root are less effective to improve efficiency. Moreover, the study showed that the reduction of the wavelength was detrimental in the tip region (further confirming the fact that the increase of this parameter is efficient). Also in this case, only the efficiency was documented. This study is notable, because it showed that destructive interference between tubercles can be experienced and, under certain limits, a certain desired shape of the open water curve can be achieved by the adoption of span–wise tubercle geometry.

It has to be noted that the blade of a marine propeller is a low aspect ratio rotating wing, and marked differences on the evolution of the flow can happen with respect to high aspect ratio devices, in particular in terms of three dimensional effects (radial flow) associated to the compartmentalization of the flow as well as on the hydrodynamic interaction of the pairs of vortices with wake vorticity and the consequent alteration of the self–induced velocity. A further consideration deserves to be pointed out in case of implementations in realistic behind hull configurations. In the context of propeller–engine matching, it can be deduced from the open water results that propellers modified with tubercle require a lower revolution to provide the thrust for the

design speed (under the assumption of no variation of propulsive coefficients). As a result, the propeller is less loaded with respect to the smooth one and, hence, it would be nominally farther from cavitation phenomena (disregarding the localized modification of the flow due to tubercle to modify or control the onset/extension of cavitation volume).

3.2. Open water in oblique flow

The analysis of pure oblique flow is carried out to broaden our knowledge on the behavior of tubercles in ideal off–design conditions and weakly unsteady motion, since their performance in rotor systems (aeronautic propeller or turbines) is documented only in axial symmetric flow. The open water characteristics in pure oblique flow at $\beta = 10°$ and $\beta = 20°$, are reported in Figures 9 and 12, for $Re_c = 1.0x10^5$, and Figures 10 and 13, for $Re_c = 2.5x10^5$, with the inclusion of the in–plane loads. Consistently with the analysis in open water, the absolute variation of the thrust, torque and efficiency with respect to the baseline model is visualized in Figures 11 and 14. In order to better highlight the effect of the response of the blade, K_{Ty} and K_{Tz} are reported in terms of ratio with respect to K_T in Figures 15 and 16, while K_T and K_Q are reported in terms of percentage increase with respect to the value at $\beta = 0°$ in Figures 17–18.

In general, all the propeller models experience thrust and torque overloading and develop in–plane loads. The modified propellers develop higher thrust and torque with respect to $P0$, see in particular Figures 11 and 14. At both incidence angles and flow regimes, the behavior of the modified models resembles that in axial symmetric condition: namely, models $P1$ and $P2$ are, respectively, the most similar and different in terms of K_T and K_Q with respect to the baseline, respectively.

At $\beta = 10°$, the difference of K_T is almost constant for the range of J for models $P1$ and $P3$, while it is slightly increasing with the reduction of propeller loading for model $P2$ (low amplitude and low frequency LET). In case of K_Q, the discrepancies smoothly reduces up to $J = 0.6$ and then stabilize about a constant value. The discrepancies between the two flow regimes are most evident for $P3$ (low wavelength, low amplitude LET) and $P2$ (high wavelength, low amplitude LET) for lighter propeller loading (compare dashed and solid lines in Figure 11).

The trends of the efficiency visualized in Figure 11c highlight the different behavior of model $P1$ and $P3$ with respect to $P2$. In laminar regime (see the solid lines), the former models experience a thrust–to–torque ratio is gradually deteriorated with respect to $P0$. Conversely, $P2$ is affected by a stronger torque–to–thrust ratio with respect to the baseline model up to $J = 1.0$, and then the trend is inverted. At the highest Re_c (see the dashed lines), the gain of thrust and torque is further enhanced with respect to $P0$. In particular, propellers $P2$ and $P3$ experience a very similar behavior. On the other hand, $P1$ reproduces a constant thrust–to–torque jump with a value closer to $P0$, showing a higher efficiency with respect to the altered models for $J < 0.9$.

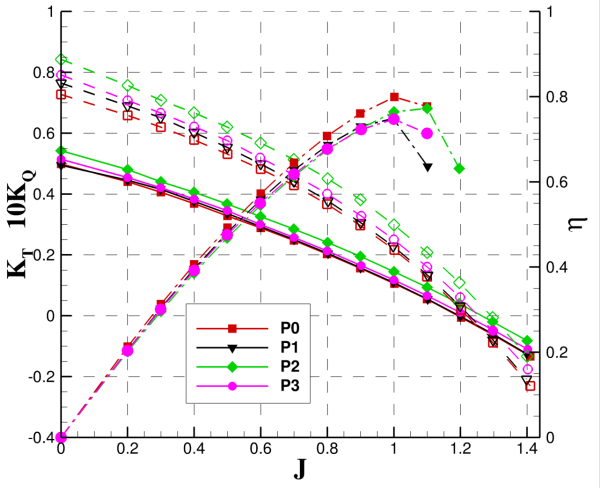

(a) Solid: K_T; dashed: $10K_Q$; dot–dashed: η

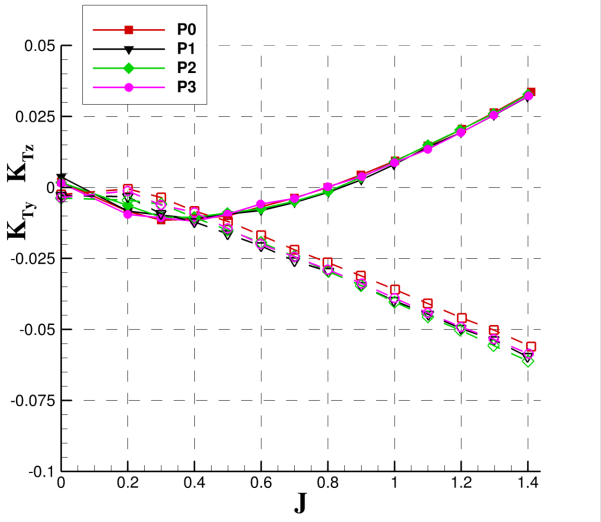

(b) solid: K_{Ty}, dashed: K_{Tz}

Figure 9: Open water characteristics, $Re_c = 1.0x10^5$, $\beta = 10^\circ$

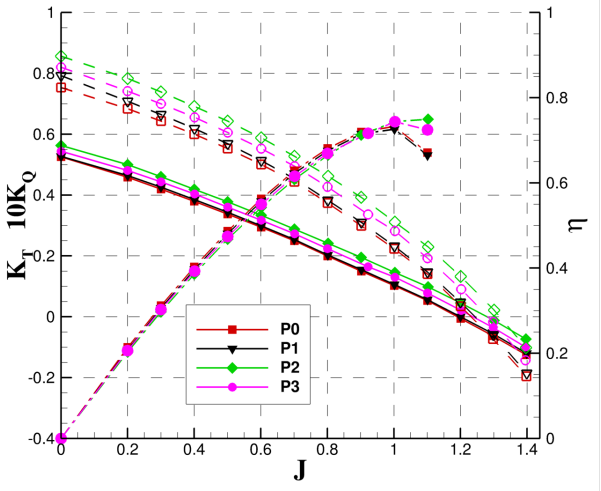

(a) Solid: K_T; dashed: $10K_Q$; dot–dashed: η

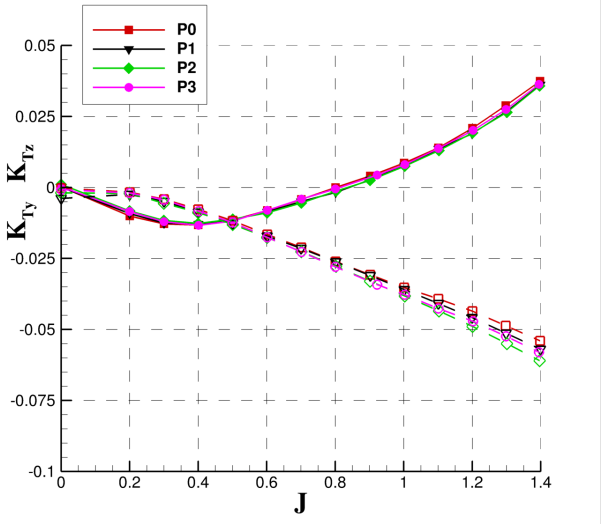

(b) solid: K_{Ty}, dashed: K_{Tz}

Figure 10: Open water characteristics, $Re_c = 2.5x10^5$, $\beta = 10^\circ$

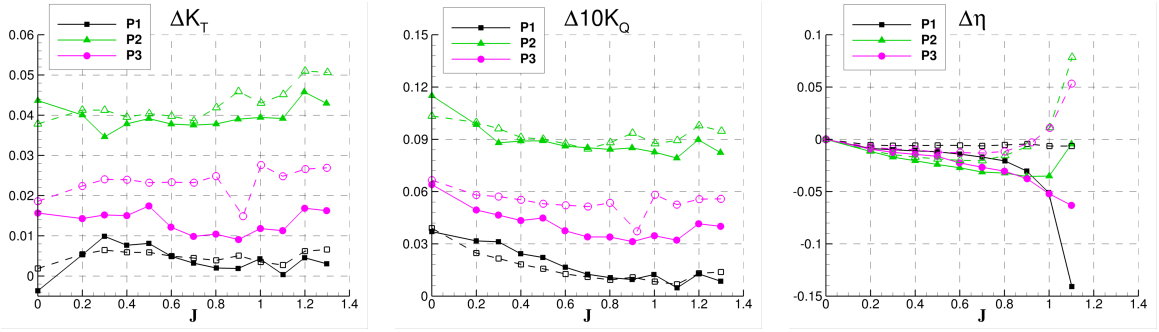

(a) Thrust (b) Torque (c) efficiency

Figure 11: Absolute discrepancy with respect to baseline propeller, $\beta = 10°$. Solid: $Re_c = 1.0x10^5$; dashed: $Re_c = 2.5x10^5$

In general, at $\beta = 20°$ the loads further increase (with respect to the axial symmetric flow) at a rate that is almost similar to the baseline propeller, see Figures 12, 13. Moreover, the comparison between 11a and 11b, and Figures 14a and 14b show that the absolute increments of K_T and K_Q with respect to $P0$ overcomes that experienced at $\beta = 10°$. Also in this case, the trends of the efficiency are sensitive to the two flow regimes investigated.

The efficiency highlights the different behavior of models $P1$ and $P3$ with respect to model $P2$, see Figure 14c. In laminar regime (see the solid lines), the thrust–to–torque ratio of the former model deteriorates with the increase of J in contrast to $P0$. Conversely, the model characterized by low amplitude and high wavelength tubercles resembles the same trend in axial symmetric condition, i.e. it overcomes the baseline in generating torque up to $J = 0.9$, and then the trend is inverted. At the higher Re_c (see the dashed lines), the gain of thrust and torque is further enhanced with respect to $P0$, in particular in case of models $P2$ and $P3$. However, in terms of efficiency, it is interesting to notice that $P2$ is not at all affected by the flow regime in contrast to the other models, in particular $P1$. In fact, the discrepancy of $P1$ is almost halved in comparison to $P2$ and, moreover, that of $P3$ is in–between the previous models up to $J = 1.0$ before experiencing an abrupt drop.

A complementary analysis of the behavior of the propellers in oblique flow and the effects of flow regime is provided in Figures 17 and 18. The Figures report the percentage increase of K_T and K_Q with respect to the value in axial symmetric condition. The propeller $P2$ experiences the smallest overloading of thrust and torque at both incidence angles. Moreover, the overloading is weakened for all the tubercled models at $\beta = 10°$. As a result, at $\beta = 20°$ the overloading of $P3$ is about 10% lower than that experienced by $P0$. It is interesting to observe that the percentage increase of K_Q at the smallest incidence is negligible for all the models, whereas the discrepancies arise at $\beta = 20°$. The overloading of thrust is almost doubled with respect to torque. At the highest Re_c, the results are qualitatively similar to the softer flow regime. However, the overloading of thrust at $\beta = 10°$ is almost halved and, hence, it is more abrupt for larger incidence. This behavior is inverted in case of torque, the overloading at the smaller incidence angle being almost doubled with respect to $Re_c = 1.0x10^5$, while remains similar at $\beta = 20°$ (compare Figures 18a and 18b).

Before discussing the result on the in–plane loads, a brief consideration on the nature of the loads monitored with the adopted set–up is deserved. The particular set–up adopted monitors in–plane moments also. A

propeller subjected to an oblique flow in the vertical plane develops also a side force that is associated to the non–homogeneous distribution of the self–induced velocity field. However, if the measuring point is taken far from the propeller plane, an additional contribution caused by the yawing moment (directly associated to the left–right asymmetry of the load caused by the incident flow) is inherently accounted for. By analogous considerations, the measure of the vertical force is affected by the pitching moment associated to the top–bottom asymmetry of the load caused by the alteration of the induced velocity. As a matter of fact, the side force associated to the induced velocity field is very small and, hence, the measure of the vertical force is close to that acting on the propeller plane. On the contrary, the side force can be strongly influenced by the yawing moment.

The in–plane forces are visualized in terms of absolute non–dimensional values in Figures 9b, 12b, 10b and 13b, and in terms of ratio with respect to thrust in Figures 15 and 16.

At both incidence angles and flow regimes, K_{Tz} increases almost linearly from heavy to lightly propeller loading condition ($0.2 < J < 1.2$), while being negligible in bollard–pull ($0 < J < 0.2$). As expected, the slope in the linear range increases with the incidence angle as a consequence of the increase of the discrepancy of the tangential force developed by the blades during the upstroke and down–stroke phase of the cycle. The vertical force is stronger for models equipped with LET: at $\beta = 10°$, the modified models are very similar among each other and differ about 10%-15% with respect to the baseline at $Re_c = 1.0x10^5$, while this difference is further contracted in the transition flow regime (see Figures 12b and 13b). At $\beta = 20°$, the trends qualitatively resembles those at the lower angle of attack, although the relative spread amplifies with the increase of the advance coefficient and with the increase of Re. The lateral force, K_{Ty} experiences a non–linear behavior: it is negative and achieve a minimum about $J = 0.4$ and then increases up to a value that is about 20% of K_{Tz} at $J = 1.0$ (at both incidences and flow regimes). The differences among the models can be appreciated only at $\beta = 20°$ for $P3$ in the heavy–to–medium propeller loading working condition. As a consequence of the higher generated thrust, the ratio of K_{Tz} and K_{Ty} is in general lower for the modified propellers in contrast to $P0$. While the ratio is comparable for heavy loading conditions, it spreads for $J > 0.8$ and $J > 1.0$ for the vertical and side force, respectively. In particular, model $P2$ is characterized by the lowest ratio of the loads at both flow regimes (see Figures 15 and 16).

It is worth noticing that at very low advance coefficients the vertical force is negligible and, consequently, the yawing moment. Therefore, the origin of the side force can be associated to asymmetries that are associated to non–homogeneous distribution of the wake at these heavy loaded conditions, plausibly triggered by destabilization modes. Moreover, it is also interesting the fact that, in contrast to different K_{Tz} and, therefore, yawing moment, all the propellers develop a similar side force. This aspect can be symptomatic of the fact that the vortex pairs generated by the tubercles can have different strength and distribution and can interact with the propeller wake system to yield the resultant induced velocity field (Stark and Shi, 2021a; Troll et al., 2021).

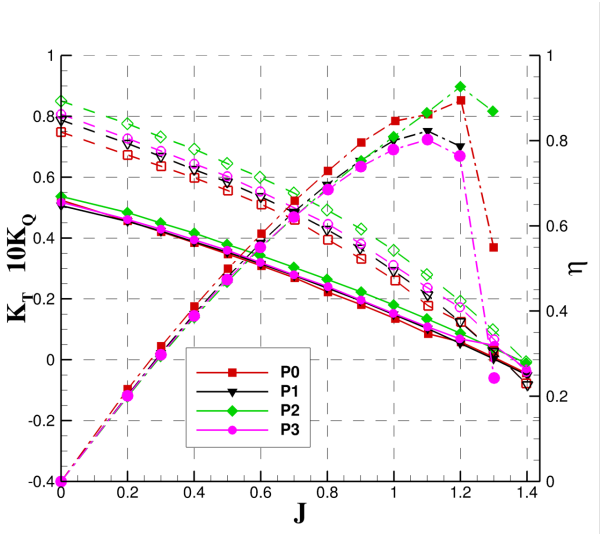

(a) open water characteristics

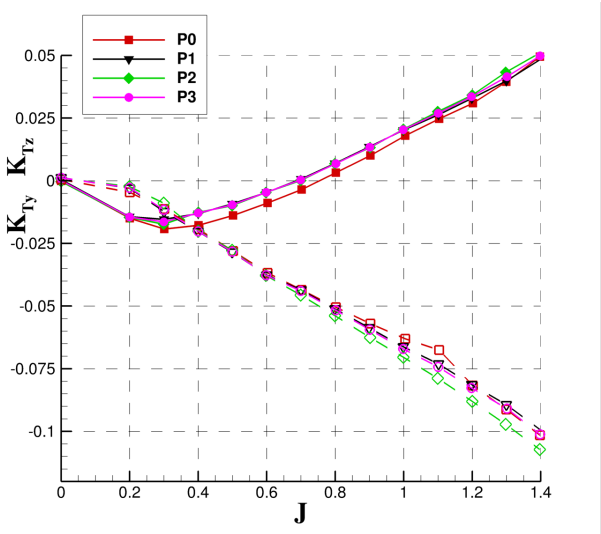

(b) solid: K_{Ty}, dashed: K_{Tz}

Figure 12: Open water characteristics, $Re_c = 1.0x10^5$, $\beta = 20°$. Solid: K_T; dashed: $10K_Q$; dot–dashed: η

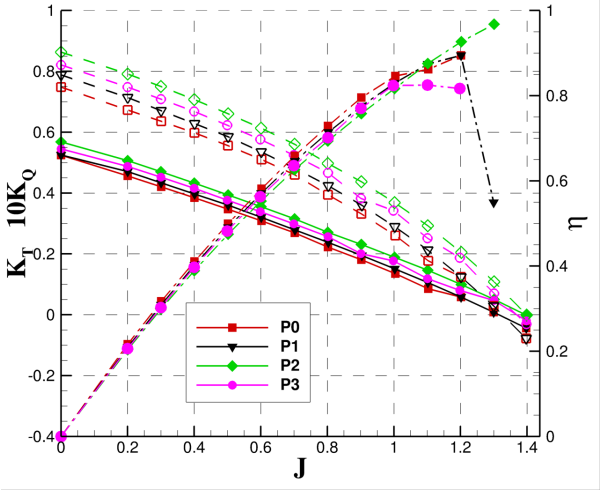

(a) solid: K_{Tx}, dashed: K_{Qx}

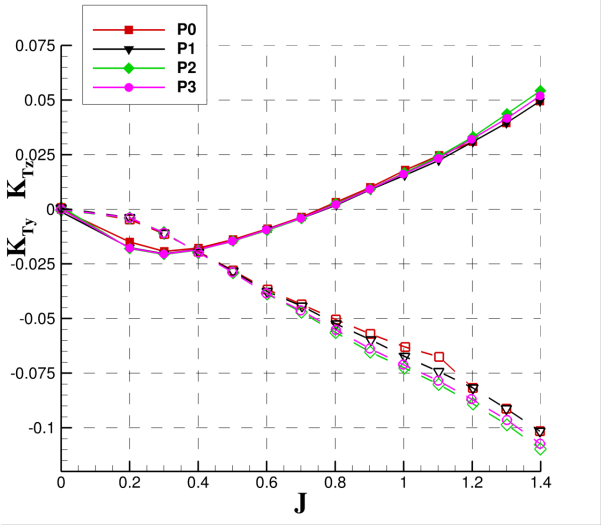

(b) solid: K_{Ty}, dashed: K_{Tz}

Figure 13: Open water characteristics, $Re_c = 2.5x10^5$, $\beta = 20°$. Solid: K_T; dashed: $10K_Q$; dot–dashed: η

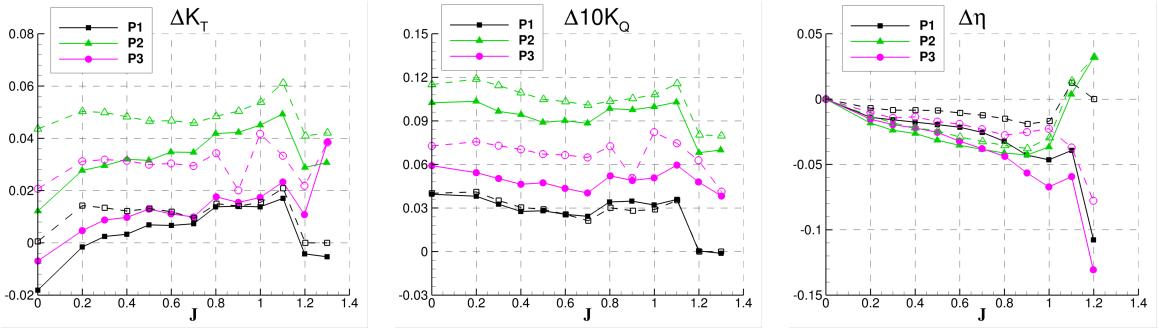

(a) Thrust (b) Torque (c) efficiency

Figure 14: Absolute discrepancy with respect to baseline propeller, $\beta = 20°$. Solid: $Re_c = 1.0x10^5$; dashed: $Re_c = 2.5x10^5$

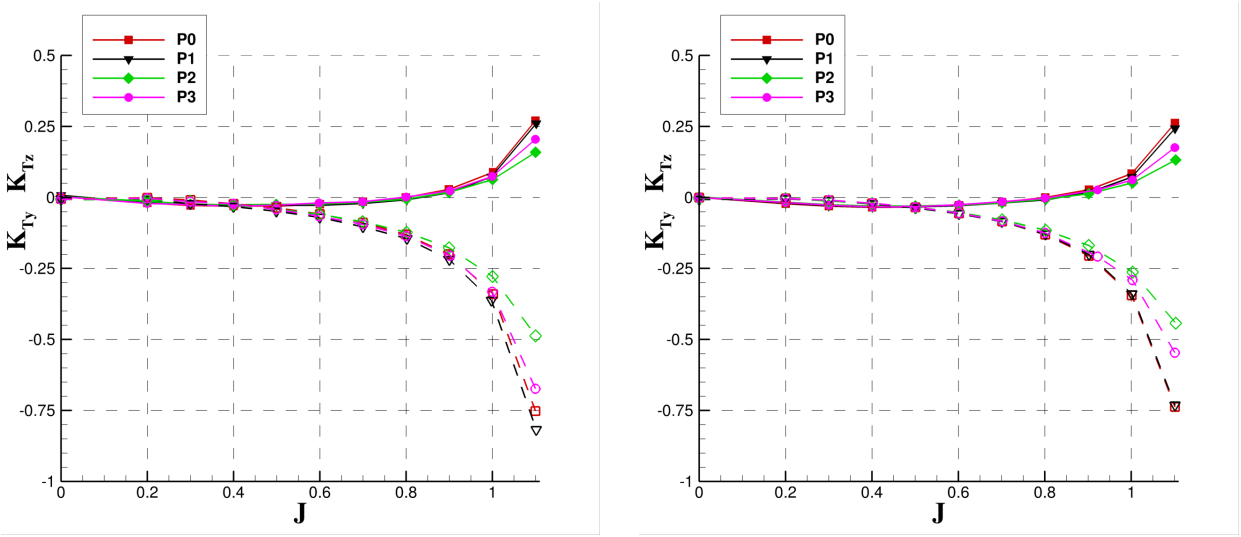

(a) $Re_c = 1.0x10^5$ (b) $Re_c = 2.5x10^5$

Figure 15: Ratio of in–plane loads, $\beta = 10°$. Solid: K_{Ty}, dashed: K_{Tz}

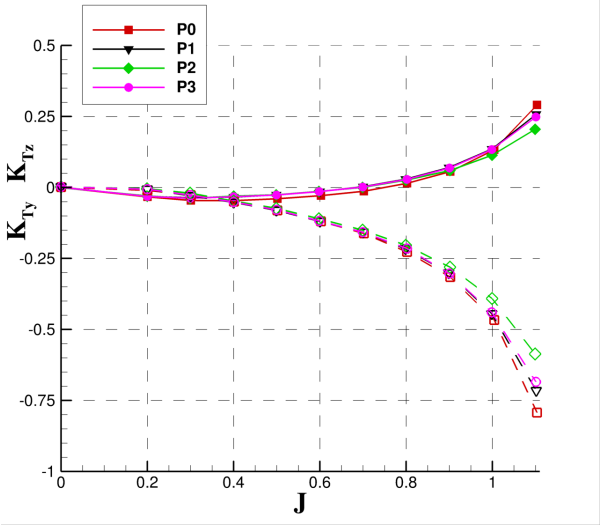

(a) $Re_c = 1.0x10^5$

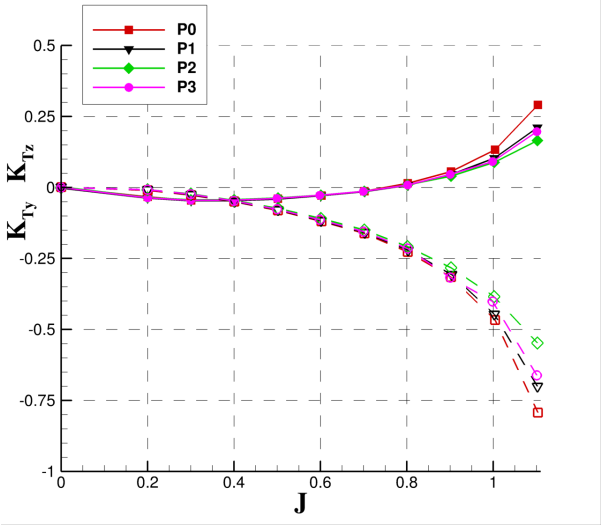

(b) $Re_c = 2.5x10^5$

Figure 16: Ratio of in–plane loads, $\beta = 20°$. Solid: K_{Ty}, dashed: K_{Tz}

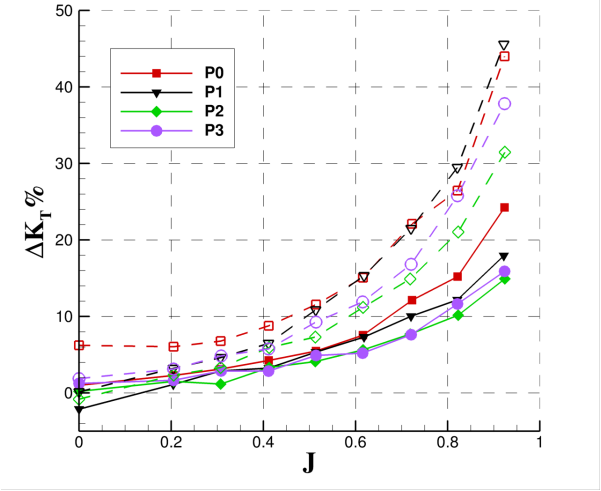

(a) $Re_c = 1.0x10^5$

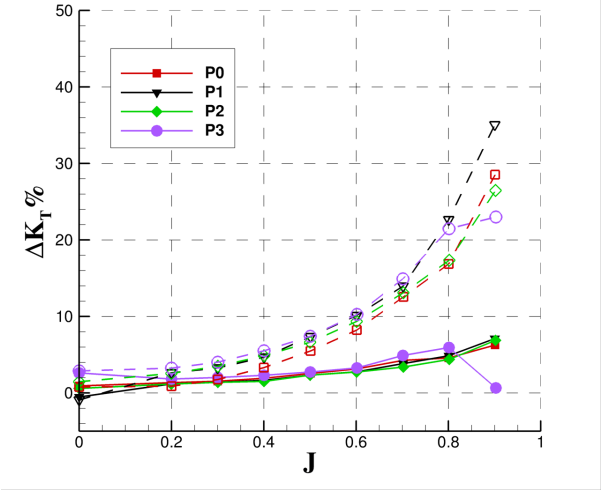

(b) $Re_c = 2.5x10^5$

Figure 17: Percentage increment of thrust. Solid: $\beta = 10°$, dashed: $\beta = 20°$

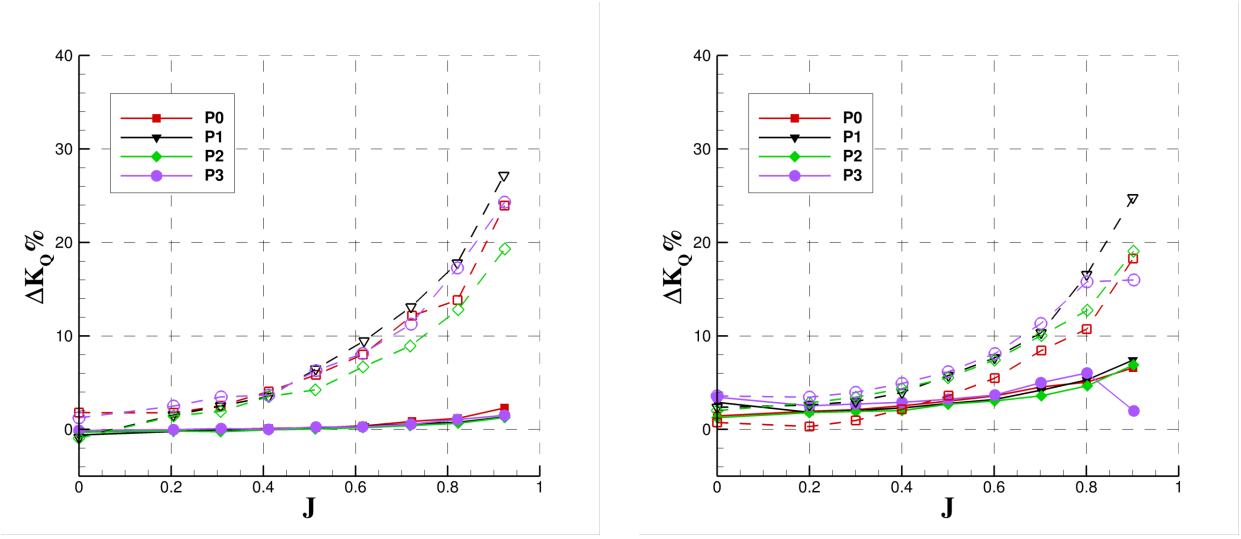

(a) $Re_c = 1.0x10^5$ (b) $Re_c = 2.5x10^5$

Figure 18: Percentage increment of torque. Solid: $\beta = 10°$, dashed: $\beta = 20°$

4. Conclusions

The present work is concerned with an experimental investigation on the effect of leading edge tubercle on the performance of a marine propeller. Three different configurations of tubercles with different amplitude and wavelength have been applied to a five bladed Wageningen B series propeller with modified NACA0012 sections. The propellers were tested at two different Reynolds numbers with the aim to range from laminar to turbulent flow. The tests conditions consisted of open water tests in axial symmetric and oblique flows up to 20° in order to investigate steady and unsteady regime at low characteristic frequency (shaft frequency) representative of off–design condition. The results refer to cavitation free condition. The key points of the present research is that the same tubercle layout, i.e. the one characterized by low amplitude and high wavelength, improved both the performance in axial symmetric condition and oblique flow. Moreover, in this two different conditions, the performance of the tubercles can be affected at a different extent by the variation of Reynolds number. A brief resume is proposed in the following.

In axial symmetric flow, all the modified propellers developed higher thrust and torque with respect to the reference geometry. The efficiency of the modified propeller is improved for $J > 0.9$, i.e. in the low loaded working regime of the propeller, while it is worsened at low advance coefficients. LET characterized by lowest amplitude and high wavelength (P2) gave rise to the largest differences with respect to the baseline. Conversely, the layout with high amplitude and high wavelength (P1) provided the smallest variations with respect to the baseline. Propeller model $P3$ was intermediate among the tubercled models. The variation of Reynolds number highlighted a different behavior associated to the LET: in case of propeller $P2$, the variation of thrust and torque were minimal, whereas for the other cases the discrepancy was larger. Interestingly, the increase of Reynolds number caused the reduction of thrust and torque for propeller $P1$ and $P2$, the opposite for propeller $P3$.

At incidence, the well known increase of thrust and torque and generation of in–plane loads were observed. The same relative discrepancy among the modified and baseline models observed in straight ahead is confirmed in terms of thrust at both incidence angles and flow regimes. This behavior is also confirmed for torque, with the exception of the incidence at $\beta = 20°$ at the highest Reynolds number, the overloading being comparable to the baseline. On the contrary, the model with high amplitude and low frequency tubercles experienced the most critical overloading at the highest incidence and similar behavior to the baseline for both thrust and torque. The overloading of thrust and torque is more sensitive to the flow regime at the lowest incidence: in fact, at $Re_c = 1.0x10^5$ the discrepancies between the models are more amplified. Moreover, the overloading is weakened with the increase of Reynolds number. It was worth of noticing that in laminar regime at $\beta = 10°$ the torque developed by all the propellers at incidence was lower with respect to the axial symmetric condition for $J < 0.6$ and this behavior was more pronounced for the tubercled geometries. Consistently with thrust and torque, the modified propellers developed stronger vertical force with respect to the baseline and with the same trends of thrust and torque (namely, propeller $P2$ was the most different one). The increase of the vertical force was almost linear with the drift angle. In terms of force–to–thrust ratio, K_{Tz} ranged to almost 10% and 30% in the range associated from rectilinear to typical maneuvering conditions ($0.6 < J < 1$). Due to the specific experimental set–up adopted, the in plane loads accounted also for the yawing and pitching moment that gave rise to a non negligible side force that resulted very similar for all the models.

5. Development of future research

The present results are obviously limited for the baseline blade shape and *LET* geometry and a definitive conclusion on its benefit is premature. It is opinion of the authors that the research in this context should be developed focusing on three different main aspects. Specifically, the measurements of the total loads developed by the propeller should be enhanced with single blade measurements and complemented with flow field measurements and visualizations. For example, cross correlation of the bending moments with the thrust can help to better understand the position a tubercle configuration is more efficient with respect to the other. Moreover, due to the possibility to inspect the variations of the loads during the period, the behavior of the tubercles during unsteady conditions such as oblique flow can be identified. In this regard, the almost equivalent values of the lateral force for all the models raise the question about the interaction of the vortex pairs generated by the tubercles and the propeller wake. Since the origin of the side force is associated to asymmetric distribution of the self–induced velocity field, the vortex pairs can play a role on the amplification/mitigation of asymmetric distribution. The characterization of the flow field in the wake of the propeller is fundamental to capture the dynamics of the vortex pairs and the mechanism they modify the vortex system of the wake and, in turns, its induced velocity field. Moreover, the effect of tubercles on the evolution of the wake is needed to draw the more as possible holistic overview on this technological solution, due to the strict implications of wake dynamics on induced vibration and noise. Moreover, since the shape of the blade of a marine propeller is optimized in the wake field of the ship, the combination of tubercles with skew, rake and camber of the sections should be

clarified. To this aim, a larger set of tubercle geometries should be considered, following the ideas proposed for aeronautic propeller (Asghar et al., 2020) and tidal turbines (Shi et al., 2016a). In this context, Computational Fluid Dynamics, once validated for a relatively small cases of *LET* configurations, could be essential to the in–depth understanding of the flow mechanisms and, in particular, cheaper with respect to experiments for testing a larger number of configurations to converge towards the optimal solutions. Finally, the real benefit of these solutions should be tested in–behind hull, possibly during mimicking realistic operative conditions (motions in waves or maneuver) and, obviously, including the effect of cavitation. The tubercles, subjected to the multi–frequency, unsteady flow field that is generated during these situations can give rise to unexpected local flow behavior, load generation and wake development in contrast to the isolated propeller. In this regard, a feasible solution could be to design test conditions specifically suited to circumscribe basic physical phenomena of the *LET* (i.e., performance in harmonic or 'synthetic' wake). This approach is also attractive for complementary numerical simulations due to reduction of computational resources.

6. Aknowledgments

The authors express their gratitude to Mr. Giampaolo Ponzo for his support in the production of the propeller series.

References

Arifin, M., Felayati, F., 2021. Numerical study of b-screw ship propeller performance: Effect of tubercle leading edge. International Journal of Marine Engineering Innovation and Research 6.

Asghar, A., Perez, R., Jansen, P., Allan, W., 2020. Application of leading-edge tubercles to enhance propeller performance. AIAA Journal 58. doi:https://doi.org/10.2514/1.J058740.

Bai, C.J., Wang, W.C., Chen, P.W., 2016. The effects of sinusoidal leading edge of turbine blades on the power coefficient of horizontal-axis wind turbine (hawt). International Journal of Green Energy 13, 1193–1200. URL: https://doi.org/10.1080/15435075.2016.1180624, doi:10.1080/15435075.2016.1180624.

Butt, F., Talha, T., 2019. Application of leading-edge tubercles to enhance propeller performance. Journal of Aircraft 56. doi:https://doi.org/10.2514/1.C034845.

Charalambous, N., Eames, I., 2019. A computational analysis of a marine propeller with tubercle and its contribution in reducing sheet cavitation, in: Proc. of 6th Symposium on Marine Propulsors, SMP19, Rome, Italy.

Custodio, D., Henoch, C., Johari, H., 2018. Cavitation on hydrofoils with leading edge protuberances. Ocean Engineering 162, 196–208. URL: https://www.sciencedirect.com/science/article/pii/S0029801818308229, doi:https://doi.org/10.1016/j.oceaneng.2018.05.033.

Dubbioso, G., Muscari, R., Ortolani, F., Di Mascio, A., 2020. Numerical analaysis of marine propellers low frequency noise during maneuvering. Applied Ocean Research 71, 399–419.

Dubbioso, G., Ortolani, F., 2020. Analysis of fretting inception for marine propeller by single blade loads measurement in realistic operating conditions. straight ahead and turning circle maneuver. Marine Structures 71, 102720. URL: https://www.sciencedirect.com/science/article/pii/S0951833920300149, doi:https://doi.org/10.1016/j.marstruc.2020.102720.

Fish, F., Battle, J., 1995. Hydrodynamic design of humpback whale flippers. Journal of Morphology 225, 51–60.

Fish, F.E., 2020. Advantages of aquatic animals as models for bio-inspired drones over present AUV technology. Bioinspiration & Biomimetics 15, 025001. URL: https://doi.org/10.1088/1748-3190/ab5a34, doi:10.1088/1748-3190/ab5a34.

Grigoropoulos, G., Campana, E., Diez, E., Serani, A., Goren, O., Sarioz, K., Danisman, D., Visonneau, M., Queutey, P., Abdel-Maksoud, M., Stern, F., 2017. Misson–based hull form and propeller optimization of a transom stern destroyer for best performance in the sea environment, in: Proc. of 7$^{\text{th}}$ MARINE, Nantes, France.

Hrynuk, J.T., Bohl, D.G., 2020. The effects of leading-edge tubercles on dynamic stall. Journal of Fluid Mechanics 893, A5. doi:10.1017/jfm.2020.216.

Ianniello, S., Muscari, R., Di Mascio, A., 2014. Ship underwater noise assessment by the Acoustic Analogy. Part II: hydroacoustic analysis of a ship scaled model. Journal of Marine Science and Technology 19, 52–74.

Ibrahim, I., New, T., 2015a. A numerical study on the effects of leading edge modifications upon propeller performance, in: Proc. of 9$^{\text{th}}$ International Symposium on Shear Flow and Turbulence, Melbourne, Australia.

Ibrahim, I., New, T., 2015b. Flow Separation Control of Marine Propeller Blades through Tubercle Modifications, in: Proc. of 10$^{\text{th}}$ South Pacific Conference on Flow Visualization and Image Processing, Naples, Italy.

Ibrahim, M., Alsultan, A., Shen, S., Amano, R.S., 2015. Advances in Horizontal Axis Wind Turbine Blade Designs: Introduction of Slots and Tubercle. Journal of Energy Resources Technology 137. URL: https://doi.org/10.1115/1.4030399, doi:10.1115/1.4030399.

ITTC, 2014. Quality System Manual-Recommended procedures and guidelines. Technical Report 7.5-0.2-0.3-0.2.1. 27nd International Towing Tank Conference (ITTC).

Joshi, A., Kulkarni, A., Joshi, G., 2020. Computational Study of Leading Edge Tubercles on Propeller Performance, in: Proc. of the International Conference on Recent Advances in Computational Techniques (ICRACT) 2020.

Kant, R., Bhattacharyya, A., 2020. A bio-inspired twin-protuberance hydrofoil design. Ocean Engineering 218, 108209. URL: https://www.sciencedirect.com/science/article/pii/S0029801820311355, doi:https://doi.org/10.1016/j.oceaneng.2020.108209.

Ke, W., Hashem, I., Zhang, W., Zhu, B., 2022. Influence of leading-edge tubercles on the aerodynamic performance of a horizontal-axis wind turbine: A numerical study. Energy 239, 122186. URL: https://www.sciencedirect.com/science/article/pii/S0360544221024348, doi:https://doi.org/10.1016/j.energy.2021.122186.

Lacagnina, G., Chaitanya, P., Kim, J.H., Berk, T., Joseph, P., Choi, K, S., Ganapathisubramani, B., Hasheminejad, S., Chong, T., Stalnov, O., Shahab, M., Omidyeganeh, M., Pinelli, A., 2021. Leading edge serrations for the reduction of aerofoil self-noise at low angle of attack, pre-stall and post-stall conditions. International Journal of Aeroacoustics 20, 130–156. doi:10.1177/1475472X20978379.

Lau, A.S., Haeri, S., Kim, J.W., 2012. Reduction of flow induced airfoil tonal noise using leading edge sinusoidal modifications. Acoustic Australia 40, 172–177.

Lau, A.S., Haeri, S., Kim, J.W., 2013. The effect of wavy leading edges on aerofoil–gust interaction noise. Journal of Sound and Vibration 332, 6234–6253. URL: https://www.sciencedirect.com/science/article/pii/S0022460X13005713, doi:https://doi.org/10.1016/j.jsv.2013.06.031.

Li, D., Yang, Q., Yang, W., Chang, H., Wang, H., 2021. Bionic leading-edge protuberances and hydrofoil cavitation. Physic of Fluids 33, 093317. doi:https://doi.org/10.1063/5.0069587.

Li, Z., Qian, Z., Ji, B., 2020. Transient cavitating flow structure and acoustic analysis of a hydrofoil with whale-like wavy leading edge. Applied Mathematical Modelling 85, 60–88. URL: https://www.sciencedirect.com/science/article/pii/S0307904X20301876, doi:https://doi.org/10.1016/j.apm.2020.04.004.

Miklosovic, D., Murray, M., Howle, L., 2007. Experimental evaluation of sinusoidal leading edges. Journal of Aircraft 44, 1404–1408. doi:10.2514/1.30303.

Miklosovic, D., Murray, M., Howle, L., Fish, F., 2004. Leading-edge tubercles delay stall on humpback whale (megaptera novaeangliae) flippers. Physics of Fluids 16, L39–L42. doi:10.1063/1.1688341.

Naveen, K., Kiran, S., Kumar, K., 2018. Design and analysis of marine propellers with leading edge tubercles. International Journal for Research in Applied Science & Engineering Technology 6.

Ortolani, F., Dubbioso, G., 2019a. Experimental investigation of blade and propeller loads: steady turning motion. Applied Ocean Resesarch 91, 101874.

Ortolani, F., Dubbioso, G., 2019b. Experimental investigation of blade and propeller loads: straight ahead motion. Applied Ocean Resesarch 87, 111–129.

Ortolani, F., Dubbioso, G., Muscari, R., Mauro, S., Di Mascio, A., 2018. Experimental and numerical investigation of propeller loads in off-design conditions. Journal of Marine Science and Engineering 6, 45–68.

Ortolani, F., Mauro, S., Dubbioso, G., 2015. Investigation of the radial bearing force developed during actual ship operations. part 1: Straight ahead sailing and turning maneuvers. Ocean Engineering 94, 67 – 87. doi:http://dx.doi.org/10.1016/j.oceaneng.2014.11.032.

Pedro, H., Kobayashi, M., 2008. Numerical Study of Stall Delay on Humpback Whale Flippers. doi:10.2514/6.2/008-584.

Petrin, C., Martin, T., Caire, W., Thies, M., Elbing, B., 2018. Modification of drag on the ear of Brazilian free-tailed bats (Tadarida brasiliensis) via leading-edge tubercles, in: AIAA Aviation and Aeronautics Forum and Exposition, FD-09 Bio-Inspired Fluid Dynamics, Atlanta, June 25-29.

Shanmukha Srinivas, K., Datta, A., Bhattacharyya, A., Kumar, S., 2018. Free-stream characteristics of bio-inspired marine rudders with different leading-edge configurations. Ocean Engineering 170, 148–159. URL: https://www.sciencedirect.com/science/article/pii/S0029801818304190, doi:https://doi.org/10.1016/j.oceaneng.2018.10.010.

Shi, W., Atlar, M., Norman, R., Aktas, B., Turkmen, S., 2016a. Numerical optimization and experimental validation for a tidal turbine blade with leading-edge tubercles. Renewable Energy 96, 42–55. URL: https://www.sciencedirect.com/science/article/pii/S0960148116303664, doi:https://doi.org/10.1016/j.renene.2016.04.064.

Shi, W., Atlar, M., Norman, R., Day, S., Aktas, B., 2019a. Effect of waves on the leading-edge undulated tidal turbines. Renewable Energy 131, 435–447. URL: https://www.sciencedirect.com/science/article/pii/S0960148118308693, doi:https://doi.org/10.1016/j.renene.2018.07.072.

Shi, W., Atlar, M., Norman, R., Day, S., Aktas, B., 2019b. Effect of waves on the leading-edge undulated tidal turbines. Renewable Energy 131, 435–447. URL: https://www.sciencedirect.com/science/article/pii/S0960148118308693, doi:https://doi.org/10.1016/j.renene.2018.07.072.

Shi, W., Rosli, R., Atlar, M., Norman, R., Wang, D., Yang, W., 2016b. Hydrodynamic performance evaluation of a tidal turbine with leading-edge tubercles. Ocean Engineering 117, 246–253. URL: https://www.sciencedirect.com/science/article/pii/S0029801816300221, doi:https://doi.org/10.1016/j.oceaneng.2016.03.044.

Shin, Y.J., Kim, M.C., Lee, J.H., Song, M.S., 2019. A numerical and experimental study on the performance of a twisted rudder with wavy configuration. International Journal of Naval Architecture and Ocean Engineering 11, 131–142. URL: https://www.sciencedirect.com/science/article/pii/S2092678217303370, doi:https://doi.org/10.1016/j.ijnaoe.2018.02.014.

Stanway, M., 2008. Hydrodynamic effects of leading-edge tubercles oncontrol surfaces and in flapping foil propulsion.

Stark, C., Shi, W., 2021a. Hydroacoustic and hydrodynamic investigation of bio-inspired leading-edge tubercles on marine-ducted thrusters. Royal Society Open Science 8, 210402. doi:https://http://doi.org/10.1098/rsos.210402.

Stark, C., Shi, W., 2021b. The influence of leading edge tubercles on the sheet cavitation development of a benchmark marine propeller, in: Proc. of ASME 2021 40$^{\text{th}}$ International Conference on Ocean, Offshore and Arctic Engineering, OMAE2021, Virtual.

Stark, C., Shi, W., Atlar, M., 2021a. A numerical investigation into the influence of bio-inspired leading-edge tubercles on the hydrodynamic performance of a benchmark ducted propeller. Ocean Engineering 237, 109593. URL: https://www.sciencedirect.com/science/article/pii/S002980182100977X, doi:https://doi.org/10.1016/j.oceaneng.2021.109593.

Stark, C., Shi, W., Troll, M., 2021b. Cavitation funnel effect: Bio-inspired leading-edge tubercle application on ducted marine propeller blades. Applied Ocean Research 116, 102864. URL: https://www.sciencedirect.com/science/article/pii/S0141118721003357, doi:https://doi.org/10.1016/j.apor.2021.102864.

Troll, M., Shi, W., Stark, C., 2021. The Influence of Leading-Edge Tubercles on Wake Flow Dynamics of a Marine Rudder, in: Proc. of 9$^{\text{th}}$ International conference on Computational Methods in Marine Engineering (MARINE 2021), June 2-4.

Weber, P., Howle, L., Murray, M., 2010. Lift, drag, and cavitation onset on rudders with leading-edge tubercles. Marine Technology 47, 27–36. doi:https://doi.org/10.5957/mtsn.2010.47.1.27.

Zhang, Bi, 2012. Aerodynamic characteristics of wind turbine blades with a sinusoidal leading edge. Wind Energy 15, 407–424. doi:https://doi.org/10.1002/we.479.

Zhang, Y., Zhang, M., Cai, C., Xu, J.Z., 2020. Aerodynamic load control on a dynamically pitching wind turbine airfoil using leading-edge protuberance method. Acta Mechanica Sinica 36, 275. URL: http://ams.cstam.org.cn/EN/abstract/article_157196.shtml, doi:10.1007/s10409-020-00939-2.

Zhu, W., Gao, H., 2021. Hydrodynamic characteristics of bio-inspired marine propeller with various blade sections. Ships and Offshore Structures 16, 156–171. doi:10.1080/17445302.2020.1713039.